Supplementary Information

Chemical templates that assemble the metal superhydrides

Yuanhui Sun and Maosheng Miao*

Department of Chemistry and Biochemistry, California State University Northridge, CA USA

*Email: mmiao@csun.edu

Supplementary Material

Section I. Energetics of H incorporated in superhydrides 3

Section II. The chemical templates in various superhydrides..... 5

Section III. The normal stresses of the metal sub-lattices in superhydrides..... 11

Section IV. The chemical templates strengths in MH_6 and MH_{10} 12

Section V. The building units of H lattices and their aromaticity 13

Section VI. The schematic of the chemical template mechanism for superhydride formation 20

Section VII. Stabilization of H units in superhydrides lattice 21

Section VIII. Charge transfers in views of chemical bonds and chemical templates..... 22

Section IX. The chemical templates and stability of mixed metal superhydrides..... 23

References..... 25

Section I. Energetics of H incorporated in superhydrides

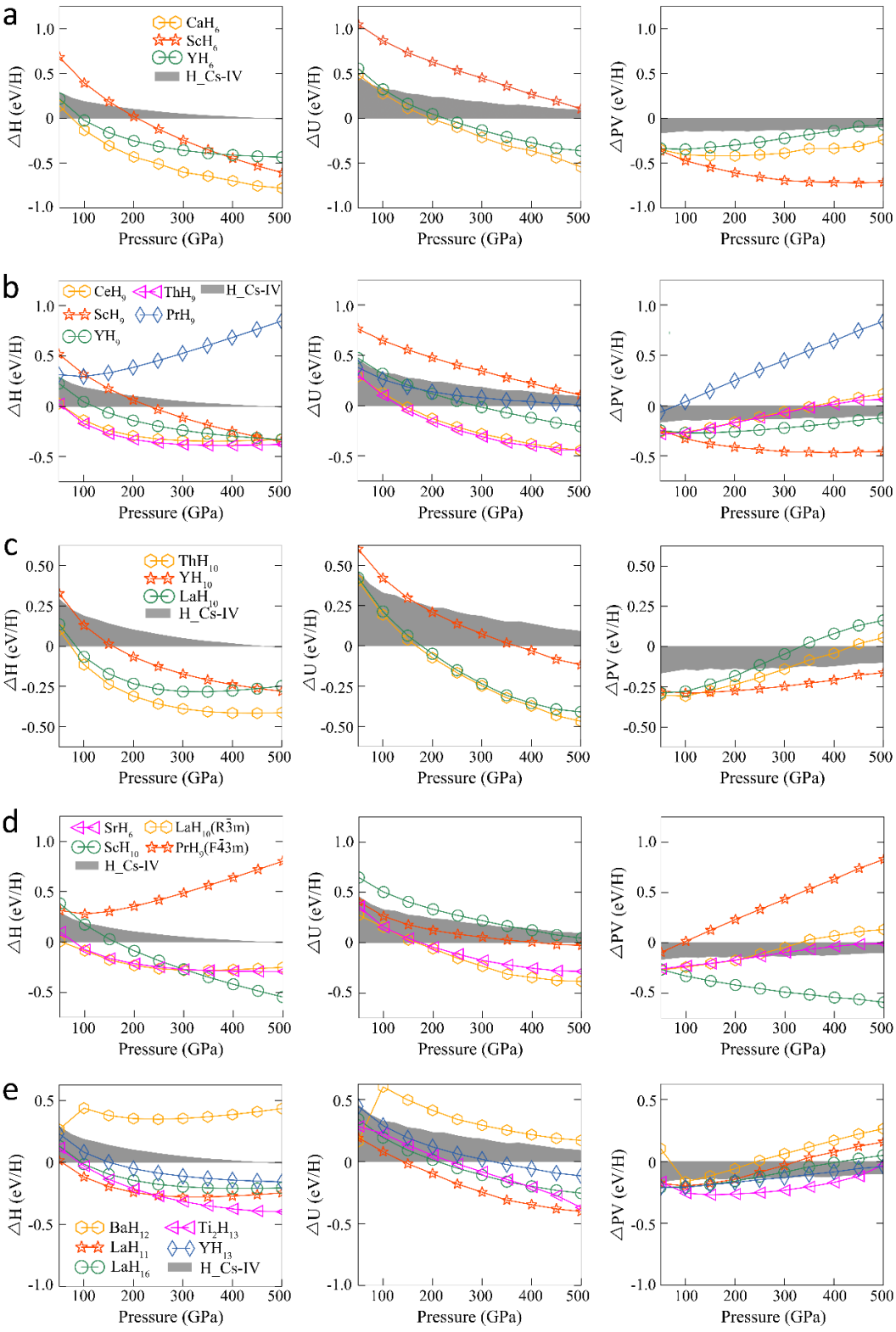

Fig. 1: The extracted enthalpy (ΔH), internal energy (ΔU) and $P\Delta V$ term of hydrogen in superhydrides relative to pristine hydrogen in molecular phase as functions of pressure. The investigated superhydrides include: **a**, CaH_6, ScH_6, YH_6, ZrH_6 in $Im\bar{3}m$ structure; **b**, CeH_9, ScH_9, YH_9, ThH_9, PrH_9 in $P6_3/mmc$ structure; **c**, ThH_{10}, YH_{10}, LaH_{10} in $Fm\bar{3}m$ structure; **d**, SrH_6 in $R\bar{3}m$ structure, ScH_{10} in $P6_3/mmc$ structure, PrH_9 in $F\bar{4}3m$ structure, LaH_{10} in $R\bar{3}m$ structure, and **e**, BaH_{12} in $Fm\bar{3}m$ structure, LaH_{11} in $P4nmm$ structure, LaH_{16} in $P6/mmm$ structure, Ti_2H_{13} in $Immm$ structure, YH_{13} in $R\bar{3}m$ structure. All quantities are relative to that of molecular H C_2/c structure. The shaded areas show ΔH, ΔU, and $P\Delta V$ of metallic H in Cs-IV structure.

Section II. The chemical templates in various superhydrides

Compound (symmetry)	Metal Lattice	Metal ELF overlay H lattice
MH_6 ($Im\bar{3}m$)	BCC M=Ca[1], Sc[2–4], Y[5,6]	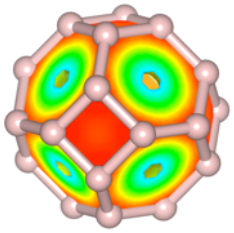
MH_{10} ($Fm\bar{3}m$)	FCC M=La[7–11], Y[10], Th[12,13]	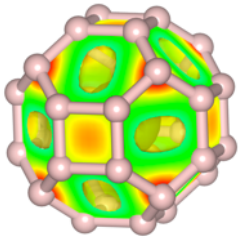
MH_9 ($P6_3/mmc$)	HCP M = Sc[10], Y[10], Th[12], Ce[14,15], Pr[16], U[17]	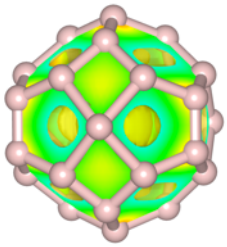
MH_6 ($R\bar{3}m$)	Hex* M = Sr[18,19]	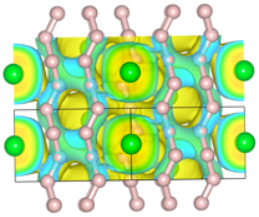
M_2H_{13} ($Immm$)	M=Ti[20]	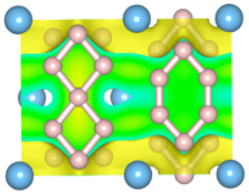
MH_9 ($F\bar{4}3m$)	FCC M=Pr[10,16], Pa[21]	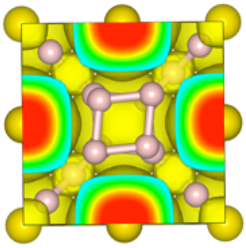
MH_{10} ($P6_3/mmc$)	HCP M= Sc[22], Zr[22], Hf[22], Lu[22]	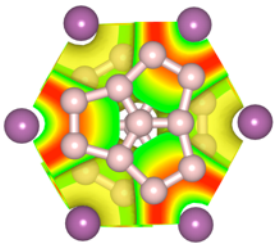
MH_{10} ($R\bar{3}m$)	Hex* M = La[8], Ac[22]	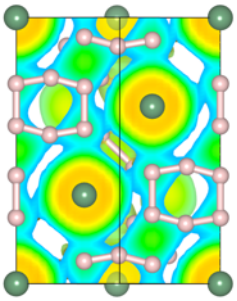
MH_{11} (P4nmm)	BCT M= La[10,23]	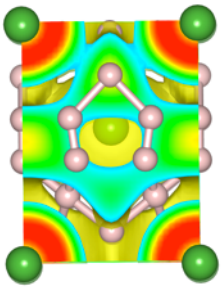
MH_{12} ($Fm\bar{3}m$)	FCC M= Ba[24]	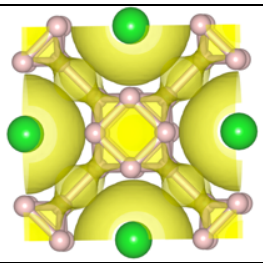
MH_{13} ($R\bar{3}m$)	FCC R-3m M=Y[10]	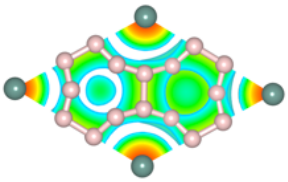
MH_{16} ($P6/mmm$)	SH M = La[23]	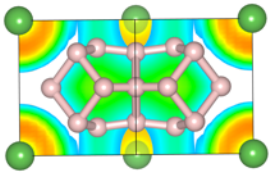

Table 1. The ELFs are calculated for metal lattices in superhydrides after removing the H atoms. The results are overlaid on H lattice. The small white balls represent H atoms, and the metal atoms, if visible, are represented by colored balls. *Hex is an FCC deformed along (111).

***$Fm\bar{3}m$* LaH_{10}.** The chemical template mechanism is based on a striking feature of superhydrides that are emerged from electronic structure calculations. It can be revealed by calculating the ELF of the metal lattices in superhydrides after removing all H atoms. For example, the La atoms form an FCC lattice in LaH_{10} superhydrides. For LaH_{10} at 300 GPa, the La lattice corresponds to an FCC La at 12.4 GPa. The ELF of this metal structure is calculated and found to have large values and maxima at octahedral and tetrahedral interstitial sites. ELF is known to reveal the chemical structure of atoms, molecules and solids. For example, it can clearly reveal the shell structure and the orbitals of heavy atoms whereas the electron density decreases monotonically with increasing radial distance. Thus, the ELF maxima at the interstitial sites of FCC La indicate that some crystal orbitals have large contributions in these regions. In other words, these crystal orbitals consist of large compositions of the local orbitals of the quasi-atoms locating at these interstitial sites. As discussed in the text, we can identify the crystal orbitals that correspond to the occupation of quasi-atom orbitals at the interstitial sites. Since the electrons do not localize completely at these interstitial sites, it is not a high-pressure electride (HPE).

The large electron distributions at the interstitial sites act as an effective chemical template for the assembly of H lattice in LaH_{10} because they match nicely with the H_{10} lattice. As shown in Fig. 2a and 2b and Supplementary Fig. 3, the H_8 cubes and the H^2 atoms of the H lattice in LaH_{10} locate exactly at the E^O and E^T interstitial sites.

***$Im\bar{3}m$* MH_6 (M=Ca, Sc, Y etc.)** The metal atoms form a BCC lattice. The ELF shows large values at the octahedral interstitial sites. Once overlaid on the H_6 lattice, it shows large values on the sites of the H atoms, especially it matches well with the H_4 and H_6 rings in the H lattice.

$P6_3/mmc$ **MH_9 (M=Ce, Y etc.)** The metal atoms form an HCP lattice. The ELF has maxima at the octahedral and tetrahedral interstitial sites. Again, it matches well with the H lattice in MH_9 superhydrides as shown in Fig. 2h and Supplementary Table 1. The H_6 corona locates at the octahedral sites whereas the two center H atoms in H_8 bipyramid units locate close to the neighboring tetrahedral sites.

$R\bar{3}m$ **MH_6 (M=Sr)** The metal atoms form a deformed FCC lattice ($R\bar{3}m$). It can be viewed as compressing an FCC lattice along the (111) diagonal direction. The ELF shows maxima at metal sites as well as the interstitial sites. With an isosurface value of 0.3, the ELF surface forms a 3D structure consisting of connected wavy chains along the perpendicular direction. Strikingly, this connected chain structure matches very well the H lattice in SrH_6, which consists of zigzag H chains. The H-H distances in the chain is 1.015 Å at 250 GPa, whereas the shortest H-H distances between the neighboring chains is 1.411 Å.

Immm **M_2H_{13} (M=Ti)** This superhydride is found to adopt a layered structure. In each layer, the H atoms form two ribbons. One ribbon consists of a chain of double-rhombus; and the other consists of isolated elongated hexagons. The H-H distances in these elongated hexagons are 1.023 and 1.048 Å. The H-H distances between two hexagons are 1.815 Å, ruling out the connection by a covalent bond. In contrast, the H-H distance between the double-rhombus is only 0.865 Å, indicating the presence of H_2 molecules. This ribbon can also be viewed as connected H_2 molecules and square planar H_5 units. Despite the complicated structure of H lattice, it matches very well the ELF maxima of the metal lattice. As shown in Supplementary Table 1, the ELF also show layered feature. Especially, it shows large values in the regions

where the double-rhombus and the elongated H_6 hexagons locate. Interestingly, the locations of the H_2 molecules correspond to regions of minimum ELF.

***$F\bar{4}3m$* MH_9 (M=Pr)** The structures can be viewed as a deformed LaH_{10} structure. Although the symmetry is lower than that of MH_{10}, the metal lattice maintains an FCC structure. Therefore, its ELF is the same as in MH_{10}, and show maxima at both the octahedral and the tetrahedral interstitial sites. There are two major differences between the H_9 lattice in this compound and the H_{10} lattice in MH_{10}. First, half of the H^2 atoms are replaced by H_4 tetrahedrons at the tetrahedral sites. Second, the H_8 cubes are deformed to match the lower symmetry caused by the replacement of H^2 atoms by H_4 tetrahedrons. Nevertheless, the H_9 lattice matches well with the ELF, with deformed H_8 cubes locating at the octahedral sites and the H^2 atoms and H_4 tetrahedrons occupying the tetrahedral sites.

***$P6_3/mmc$* MH_{10} (M=Sc, Zr, Lu, Hf etc.)** Different to other MH_{10} superhydrides, these compounds adopt a hexagonal layered structure ($P6_3/mmc$). Each layer contains 1 metal atom and 10 H atoms positions in a hexagonal lattice. Another important feature is that the H in these compounds do not form extended covalent network. Instead, they form H_{10} planar molecules with the same geometry of acepentalene ($C_{10}H_6$). The metal lattice is an HCP reduced in perpendicular direction. The ELF of this metal lattice shows rings of large value maxima locating at the B sites (if the metals locate at A sites). The highest values at the interstitial regions are as large as 0.65 for Sc. The H_{10} molecule locate in between the ELF rings, with three of its edges (2 H atoms) locating in the high ELF value region, and the H atoms sharing two pentagons locating in the medium ELF value regions. The center H atoms locate at ELF minima.

***$R\bar{3}m$* MH_{10} (M=Ac etc.)** The metal lattice of this superhydride is very close to an FCC lattice. It is slightly compressed along the (111) diagonal direction. The M-M distances inside the [111] layer are 3.688 Å whereas the M-M distances between neighboring layers are 3.497 Å. Nevertheless, the H lattice is very different to cubic MH_{10}. It is a semi-layered structure. The in-layer H-H distances are 1.085 and 1.099 Å, whereas the shortest H-H distances between layers are 1.313 Å. Despite the complex structure of H lattice, it matches well with the ELF. Similar to the ELF of an FCC structure, the ELF results of the metals in these compounds also show maxima in the octahedral and the tetrahedral interstitial sites. A deformed H_8 cube locates at each octahedral site, and one H atom occupies each tetrahedral site.

***P4nmm* MH_{11} (M=La etc.)** The metal atoms form a body-centered tetragonal (BCT) lattice. The lattice parameters at 100 GPa are a=b=3.873 Å and c=5.272 Å. The major interstitial sites are octahedral and locate at the base center. ELF of BCT La shows maxima at these sites. The H lattice matches fairly well with the ELF distribution.

***$Fm\bar{3}m$* MH_{12} (M=Ba etc.)** This type of superhydrides has the same symmetry group ($Fm\bar{3}m$) as cubic LaH_{10}. Therefore, its metal atoms form an FCC lattice. The ELF shows maxima at both the octahedral and interstitial sites. The major difference is the H lattice. The H lattice in MH_{12} consists of H_{12} cuboctahedrons (polyhedrons with 12 vertices). They all locate at the octahedral sites of the metal FCC lattice. There is no H atom locating at the tetrahedral sites.

***$R\bar{3}m$* MH_{13} (M=Y etc.)** Similar to all other $R\bar{3}m$ superhydrides (MH_6 and MH_{10}), the metal atoms form a deformed FCC by compressing the lattice along (111) diagonal direction. The H lattice shows a very unusual structural feature. Among the 13 H atoms, 12 of them locate in the

same layer with the metal atom, forming a large ring circling the metal atom. The H-H distances in the ring are 1.025 Å for YH_{13} under 200 GPa, the shortest H-H distance between rings is 1.224 Å. One extra H locates between the two layers and at the center site among three H_{12} rings, and connects them with a H-H distance of 1.210 Å. The high value regions of ELF match the H lattice including the H_{12} rings in the layers and the H atoms connecting the rings.

***P6/mmm* MH_{16} (M=La)** The metal atoms in this superhydrides form a simple hexagonal (SH) lattice. The lattice parameters for both MH_{16} at 150 GPa and the corresponding SH lattice are a=b=3.692 Å and c=3.707 Å. The H lattice consists of layers. Each layer is formed by connecting H_{14} cages by their 3 H_4 rhombus sides. There are three H-H distances inside each H_{14} cage that are 1.074, 1.011 and 1.271 Å. The minimum H-H distance between two neighboring layers is 1.525 Å. The ELF of the metal lattice show maxima at the two interstitial sites centered at the B and C sites of hexagonal lattice (assuming the metal atoms locate at the A sites) and at the center of the two metal layers. It matches very nicely with the H lattice. Each H_{14} cage centers at an interstitial site.

Section III. The normal stresses of the metal sub-lattices in superhydrides

	Com-pounds	Press-ure (GPa)	Metal Lattice Pressure (GPa)				Com-pounds	Press-ure (GPa)	Metal Lattice Pressure (GPa)		
MH_6 ($Im\bar{3}m$)	CaH_6	300	56.2	56.2	56.2	MH_{10} ($P6_3/mmc$)	ScH_{10}	300	9.3	9.3	30.7
	ScH_6	300	37.0	37.0	37.0		ZrH_{10}	300	6.5	6.5	26.7
	YH_6	300	45.8	45.8	45.8		LuH_{10}	300	13.8	13.8	49.4
							HfH_{10}	300	5.2	5.2	33.7
MH_{10} ($Fm\bar{3}m$)	LaH_{10}	300	12.4	12.4	12.4	MH_{10} ($R\bar{3}m$)	LaH_{10}	150	2.1	2.1	4.7
	YH_{10}	300	16.4	16.4	16.4		AcH_{10}	200	11.3	11.3	18.7
	ThH_{10}	300	10.1	10.1	10.1						
MH_9 ($P6_3/mmc$)	ScH_9	300	11.0	11.0	12.0	MH_{11} (P4nmm)	LaH_{11}	100	-1.1	-1.1	-0.6
	YH_9	300	22.0	22.0	24.1						
	ThH_9	300	11.9	11.9	35.1						
	CeH_9	300	1.1	1.1	15.1						
	PrH_9	300	-3.2	-3.2	8.8						
	UH_9	300	-17.4	-17.4	-5.0						
MH_6 ($R\bar{3}m$)	SrH_6	300	49.2	49.2	59.0	MH_{12} ($Fm\bar{3}m$)	BaH_{12}	135	6.3	6.3	6.3
M_2H_{13} ($Immm$)	Ti_2H_{13}	350	23.1	-6.3	21.5	MH_{13} ($R\bar{3}m$)	YH_{13}	200	4.1	4.1	-7.7
MH_9 ($F\bar{4}3m$)	PrH_9	400	4.9	4.9	4.9	MH_{16} ($P6/mmm$)	LaH_{16}	150	-3.5	-3.5	-3.4
	PaH_9	300	-1.2	-1.2	-1.2						

Table 2. Normal stresses of the metal lattices (after removing all H atoms) in superhydrides under certain pressures.

Section IV. The chemical templates strengths in MH_6 and MH_{10}

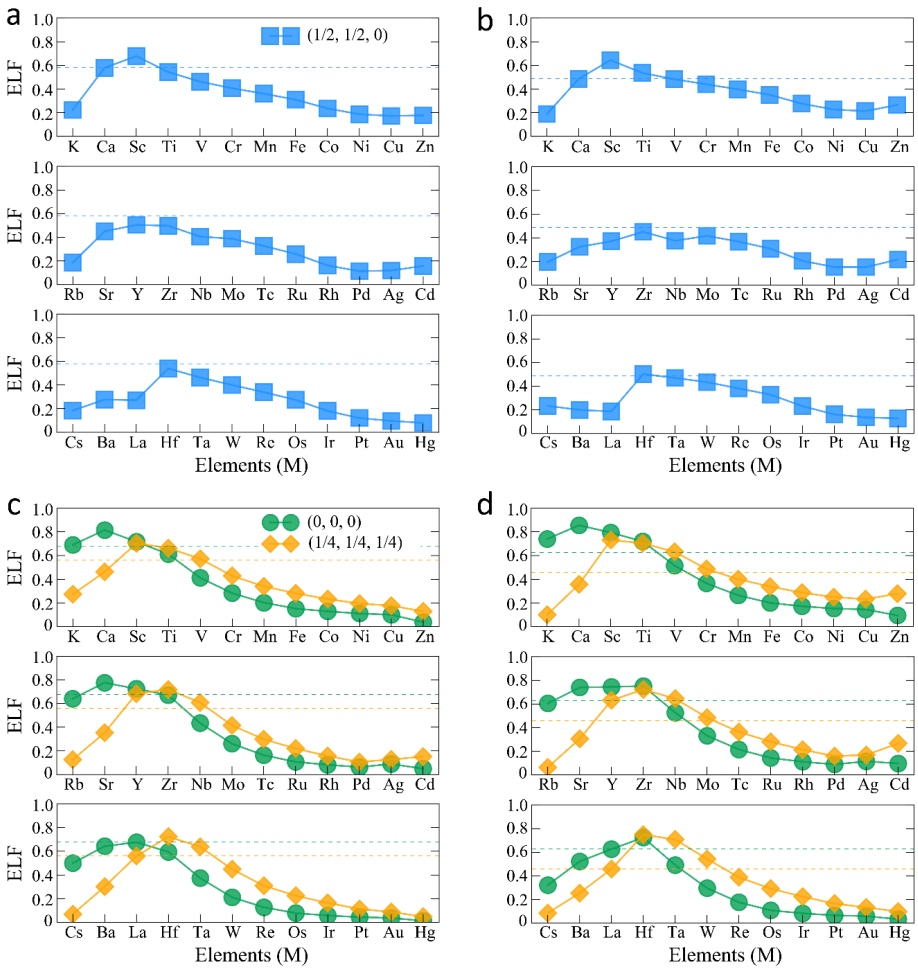

Fig. 2: The ELF values at the interstitial points for MH_6 and MH_{10}. a, The ELF values of MH_6 superhydrides at the interstitial point (1/2, 1/2, 0) at 100 GPa. M is a 4th, 5th, and 6th row metal element, respectively. **b**, The ELF values of MH_6 superhydrides at the interstitial point (1/2, 1/2, 0) at 300 GPa. The blue dashed lines in both (**a**) and (**b**) panels show the ELF values of Ca for comparison. **c**, The ELF values of MH_{10} superhydrides at the interstitial points at 100 GPa, including (0,0,0) and (1/4, 1/4, 1/4). M is a 4th, 5th, and 6th row metal element, respectively. **d**, The ELF values of MH_{10} superhydrides at the interstitial points at 300 GPa, including (0,0,0) and (1/4, 1/4, 1/4). The green and orange dashed lines show the ELF values of La at (0, 0, 0) and (1/4, 1/4, 1/4) for comparison.

Section V. The building units of H lattices and their aromaticity

Name	Compounds	Structure	Wavefunction	Energy Levels
H_4 tetrahedron	MH_9 M=Pr[10,16], Pa[21]		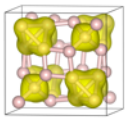 #9	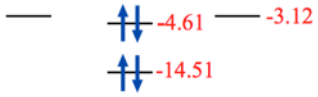 -4.61 -3.12 -14.51
H_6 hexagon	MH_6 M=Ca[1], Sc[2–4], Y[5,6]	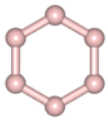	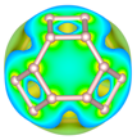 #4	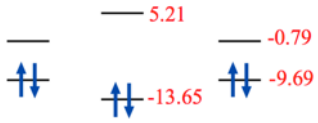 5.21 -0.79 -13.65 -9.69
H_6 corona	MH_9 M = Sc[10], Y[10], Th[12], Ce[14,15], Pr[16], U[17]		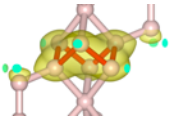 #2	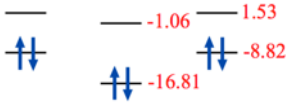 -1.06 1.53 -8.82 -16.81
H_8 cube	MH_{10} M=La[7–11], Y[10], Th[12,13]	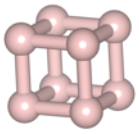	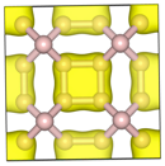 #2	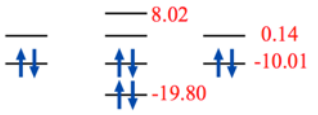 8.02 0.14 -10.01 -19.80
H_8 deformed cube	MH_9 M=Pr[10,16], Pa[21]		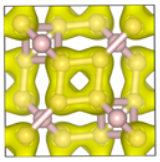 #13	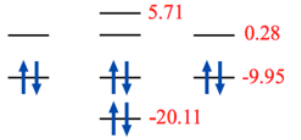 5.71 0.28 -9.95 -20.11
H_{10} Tripentagon	MH_{10} M= Sc[22], Zr[22], Hf[22], Lu[22]	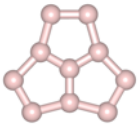	 #7	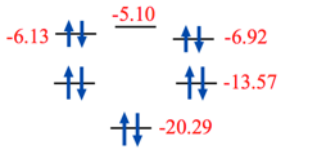 -5.10 -6.13 -6.92 -13.57 -20.29
H_{12} Cuboctahedron	MH_{12} M= Ba[24]	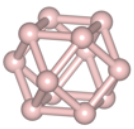	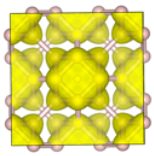 #1	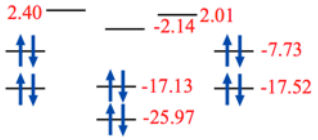 2.40 2.01 -2.14 -7.73 -17.13 -17.52 -25.97
H_{12} Ring	MH_{13} M=Y[10]	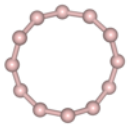	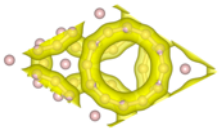	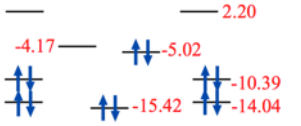 2.20 -4.17 -5.02 -10.39 -15.42 -14.04
H_{14} Cage	MH_{16} M = La[23]	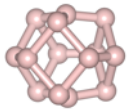		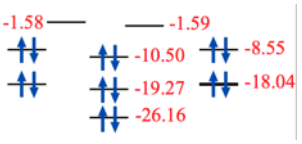 -1.58 -1.59 -10.50 -8.55 -19.27 -18.04 -26.16

Table 3. The structures and the energy levels of H clusters (building units) in superhydrides. They are identified by wavefunctions of the H lattice after removing all metal atoms in superhydrides.

Another important structure feature of the superhydrides is that their H lattices consist of building units that show unique electronic structure features, including being aromatic. Aromaticity is a concept for organic molecules consisting of conjugated π bonds formed by the p orbitals of consisting atoms. The corresponding molecular orbitals are delocalized because each p orbital can bond resonantly with two or more neighboring p orbitals. The most common examples are those formed by C 2p orbitals. Because of the topological nature of the 2p orbitals, the C atoms need to locate in the same plane in aromatic molecules or groups. The essence of the aromaticity is that the energy levels of the π orbitals form a gap, below which all the levels are occupied and above which all the level are empty. Because of the coplanar constraint, the π orbitals come in pairs except the lowest energy one that corresponds to the overall bonding state and does not contain any node. Therefore, the π systems containing 4n+2 electrons are aromatic because they fill the 2n+1 orbitals and form a gap. The size of the gap corresponds to the strength of the aromaticity, and the larger the gap, the stronger the aromacity. In contrast to π bonds, the σ bonds are usually formed by sp^n (n=3,2,1) hybrid orbitals. These bonds are localized in the region between the two bonding atoms because, each hybrid orbital can only form bond with another orbital in one direction (head to head). On the other hand, the sp^3 hybridized orbitals can form three-dimensional covalent networks, which becomes the structural framework for organic molecules and many covalent crystals.

The H-H bonds in superhydrides as well as in atomic hydrogen share the features of both the π bonds of p orbitals and σ bonds of hybrid orbitals. These bonds are formed by the 1s orbitals of two neighboring H atoms. Similar to σ bonds, they can form 3D networks as in superhydrides or in atomic hydrogen phases. On the other hand, one 1s orbital can form multiple bonds with

neighboring H atoms resonantly in a similar way as the π bonds in organic molecules. However, because the 1s orbital is spherical, the conjugation of the 1s-1s bonds does not require these bonds to be coplanar. This major difference between the H-H bonds and the C-C π bonds lifts the coplanar constraint of aromaticity. Thus, a 3D H cluster could still be aromatic, if the occupation of its energy levels satisfies the requirement of aromaticity, i.e. the lower energy orbitals are fully occupied and the higher energy orbitals are empty, forming a gap between the HOMO and the LUMO orbitals. Eventually, the aromaticity depends on the symmetry and the number of electrons of the cluster. Strikingly, we find that the H lattices of most of the superhydrides consist of building units that are aromatic. Especially, these units locate at the high value regions of ELF, often corresponding to maxima, and therefore are largely stabilized by the electrons localized in these regions. The following summarizes the most important building units found in the superhydrides that have been discovered so far.

H_4 tetrahedrons are found in $F\bar{4}3m$ MH_9 (M=Pr etc.) compounds. The four electrons fill the two lower energy orbitals and the two degenerate levels with higher energy are empty. It has a gap of 1.49 eV if the geometry parameters are taken from PrH_9 at 400 GPa. In MH_9 superhydrides, the H_4 tetrahedrons locate at the tetrahedral interstitial sites where the ELF shows maxima.

H_6 hexagons are found in $Im\bar{3}m$ MH_6 superhydrides. Many metals such as Ca, Sc, Y and La etc. can form these superhydrides. The deformed H_6 hexagons, such as elongated H_6, can be found in several other types of superhydrides, such as $Fm\bar{3}m$ MH_{10} and Immm M_2H_{13} etc. The H_6 hexagon is analogous to benzene molecules. Its aromaticity has been thoroughly discussed

previously and has been used to explain the stability of atomic hydrogen phases that consist of "graphene-like" hydrogen layered structures. The H-H distance in H_6 hexagons in LaH_6 at 300 GPa is 1.234 Å, and the corresponding HOMO-LUMO gap is found to be 8.50 eV, indicating a strong aromaticity.

H_6 corona is found in $P6_3/mmc$ MH_9 superhydrides. All 6 H atoms are equivalent. The H-H distance is 1.118 Å for CeH_9 at 300 GPa. It is also aromatic and has a large gap of 8.76 eV, similar to H_6 hexagon. Interestingly, the LUMO of H_6 corona is a single orbital, which is different to the doubly degenerate LUMO in H_6 hexagons. In MH_9 compounds, H_6 coronas locate at the octahedral interstitial sites and are significantly stabilized by the high distribution of electrons.

H_8 cube is found in $Fm\bar{3}m$ MH_{10} superhydrides. The well-known example is LaH_{10}. The H-H distances in H_8 cube in LaH_{10} at 300 GPa are 1.146 Å. This is actually longer than the H^1-H^2 distances that connect the H_8 cubes and the H^2 atoms at the tetrahedral sites. The later is 1.064 Å in LaH_{10} at 300 GPa. Still, the wavefunctions show that H_8 cube is a building unit. H_8 cube show very strong aromaticity with a gap between its HOMO and LUMO states as high as 10.15 eV. Due to the highly symmetric geometry, both HOMO and LUMO orbitals are triply degenerate. In MH_{10} superhydrides, H_8 cubes locate at the octahedral sites and are largely stabilized by the large electron localizations as revealed by the metal ELF.

Deformed H_8 cube presents in $F\bar{4}3m$ MH_9 superhydrides. It can be obtained by deforming the cube in a way that all faces become slightly bended rhombus. All H atoms are equivalent and there is only one nearest H-H distance. It has a value of 1.149 Å in PrH_9 at 400 GPa. The two

angles of the rhombus are 78.04° and 100.80°, and the dihedral angle of the bended rhombus is 11.61°. With these geometry parameters, the energy levels of the deformed H_8 cube are calculated. Despite the lowering of the symmetry, the energy levels are similar to the original H_8 cube. Especially, the HOMO and LUMO orbitals are triply degenerate. It also shows a large gap of 10.23 eV, indicating strong aromaticity. Similar to H_8 cube, the deformed H_8 cubes also locate at the octahedral sites of FCC metal lattice and are greatly stabilized by the high electron distributions in these regions.

H_{10} tripentagons are found in $P6_3/mmc$ MH_{10} superhydrides. DFT calculations predicted the formation of such compounds for several metals including Sc, Zr, Lu and Hf, etc. While concerning the H lattices, this type of superhydrides is quite unique. First, the H atoms do not form an extended covalent network. Instead, they form planar H_{10} molecules. The structure of these molecules is analogous to acepentalene ($C_{10}H_6$) and consists of three pentagons connected by sharing edges. There are three H-H distances. For ScH_{10} at 300 GPa, the H-H distance between the center H and its three neighbors (H that are shared by two neighboring pentagons) is 0.915 Å, the H-H distance between the shared H and its neighboring edge H is 1.067 Å, and the H-H diatnce between two edge H atoms is 1.007 Å. The Gaussian calculation of the electronic structure of H_{10} molecule with the same geometry as H_{10} in ScH_{10} at 300 GPa shows a small gap of 1.03 eV between its non-degenerate HOMO and LUMO levels.

H_{12} cuboctahedrons exist in $Fm\bar{3}m$ MH_{12} superhydrides. Comparing with cubic MH_{10} structure, all H atoms locate at octahedral interstitials and form cuboctahedrons. In BaH_{12} at 135 GPa, the shortest H-H distance within H_{12} is 1.271 Å, whereas the shortest H-H distance between the neighboring H_{12} is 1.344 Å. All H atoms are equivalent in cuboctahedrons. With the above

geometry, the energy levels are calculated using Gaussian program. The HOMO levels are doubly degenerate whereas the LUMO is not. The gap between the HOMO and the LUMO levels is found to be 5.59 eV, showing moderate aromaticity. Like all other H clusters, the H_{12} cuboctahedrons are also stabilized by the electron distributions at the octahedral sites in metal FCC lattices.

H_{12} ring is a striking unit found in $R\bar{3}m$ MH_{13} compounds. Its large size (3.900 Å diameter in YH_{13} at 200 GPa) and unusual shape make it difficult for close packing under high pressure. However, both the geometry and the wavefunctions distinctly reveal their existence. For YH_{13} at 200 GPa, the H-H bond length within the ring is 1.025 Å, whereas the shortest H-H distance between the rings is 1.224 Å and the shortest distance between H on the ring and the H between the layers is 1.210 Å. Different to other H units, H_{12} ring is an analogue to C π bonds, therefore should also follow the Hückel 4n+2 rule. Based on this rule, H_{12} ring is anti-aromatic, i.e. the doubly degenerate HOMO levels are half filled. However, in the YH_{13} structure, the H_{12} ring is slightly distorted. Among 12 H atoms, 6 remain in the original position, 3 move upwards and 3 downwards alternatively, creating a wave-like modulation. As the result of this deformation, a gap of 0.85 eV is opened. As discussed in the previous section, H_{12} ring matches the ELF high value regions of the metal lattice and therefore its stability is enhanced by the template effect.

H_{14} cage can be viewed as the structure unit of the H lattice in P6/mmm MH_{16} superhydrides. Not all the H atoms are equivalent and there are three different H-H distances in the cage. The H-H distance of the top H to its three neighbors (second layer) is 1.074 Å, and the H-H distance that connects the second and the third layer H atoms is 1.271 Å. Lastly, the two neighboring H atoms in the third layer has a distance of 1.011 Å. The unit is aromatic and shows a gap of 6.96

eV between its doubly degenerate HOMO levels and the single LUMO level. In MH_{16} structures, the H_{14} cages are connected by sharing the H_4 rings at its three sides, and form a 2D layered structure with hexagonal symmetry. The 2D hexagonal lattice matches well with the ELF of the metal lattice and are stabilized by the electrons localized in the region.

Section VI. The schematic of the chemical template mechanism for superhydride formation

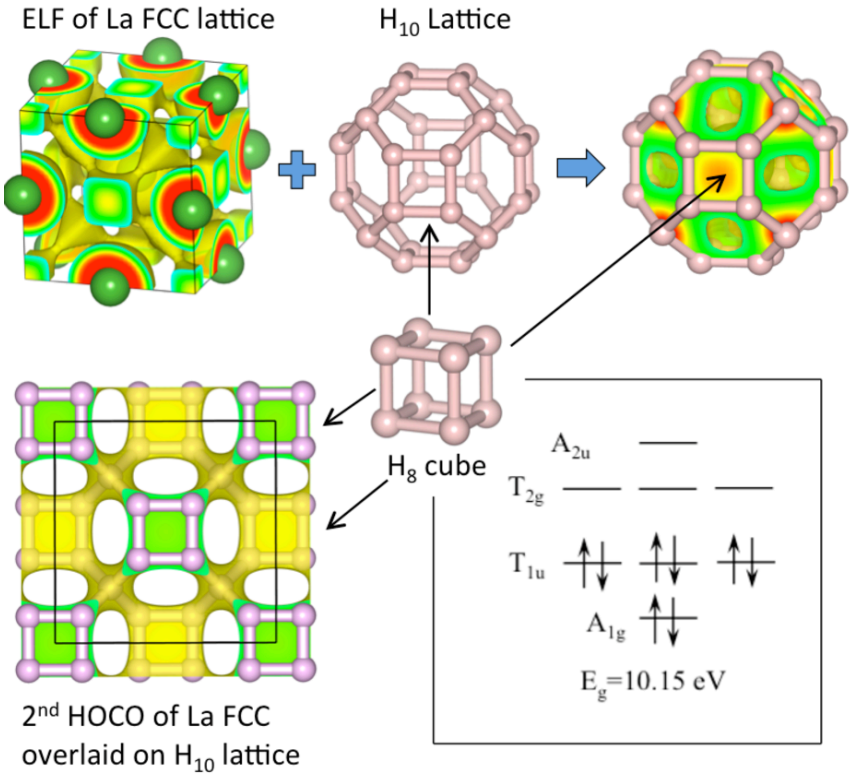

Fig. 3: The ELF of La face-centered cubic (FCC) lattice in LaH_{10} under pressure exhibits maxima at the octahedral and tetrahedral sites. It matches surprisingly well with the H_{10} lattice in LaH_{10}. Especially, the H_{10} lattice consists of H_8 cubes that locate at the octahedral interstitials of La FCC lattice, surrounding the maxima of ELF. The underlying cause of this phenomenon is the presence of the crystal orbitals of La FCC lattice that matches the H_{10} lattice. For example, the second highest occupied crystal orbital (HOCO) of La FCC at the Γ point exhibits maxima at both octahedral and tetrahedral interstitials. It interacts strongly with the H_8 cube and greatly lowers its energy relative to H_2 molecules. Furthermore, many building units of the H lattices in superhydrides are aromatic, although they are not planar. Different to C 2p orbitals, the conjugation of the H 1s orbitals does not require a planar geometry. Their aromaticity is determined by the symmetry and electron counting, and H_8 cube is aromatic and has a gap of 10.15 eV. The perfect match of the electron distribution of La lattice with the positioning of the aromatic H_8 cube significantly stabilizes the H_{10} lattice. Together with the aromaticity, this template effect drives the formation of superhydrides. The arrows in the schematic point to the locations of the H_8 cubes in H_{10} lattices.

Section VII. Stabilization of H units in superhydrides lattice

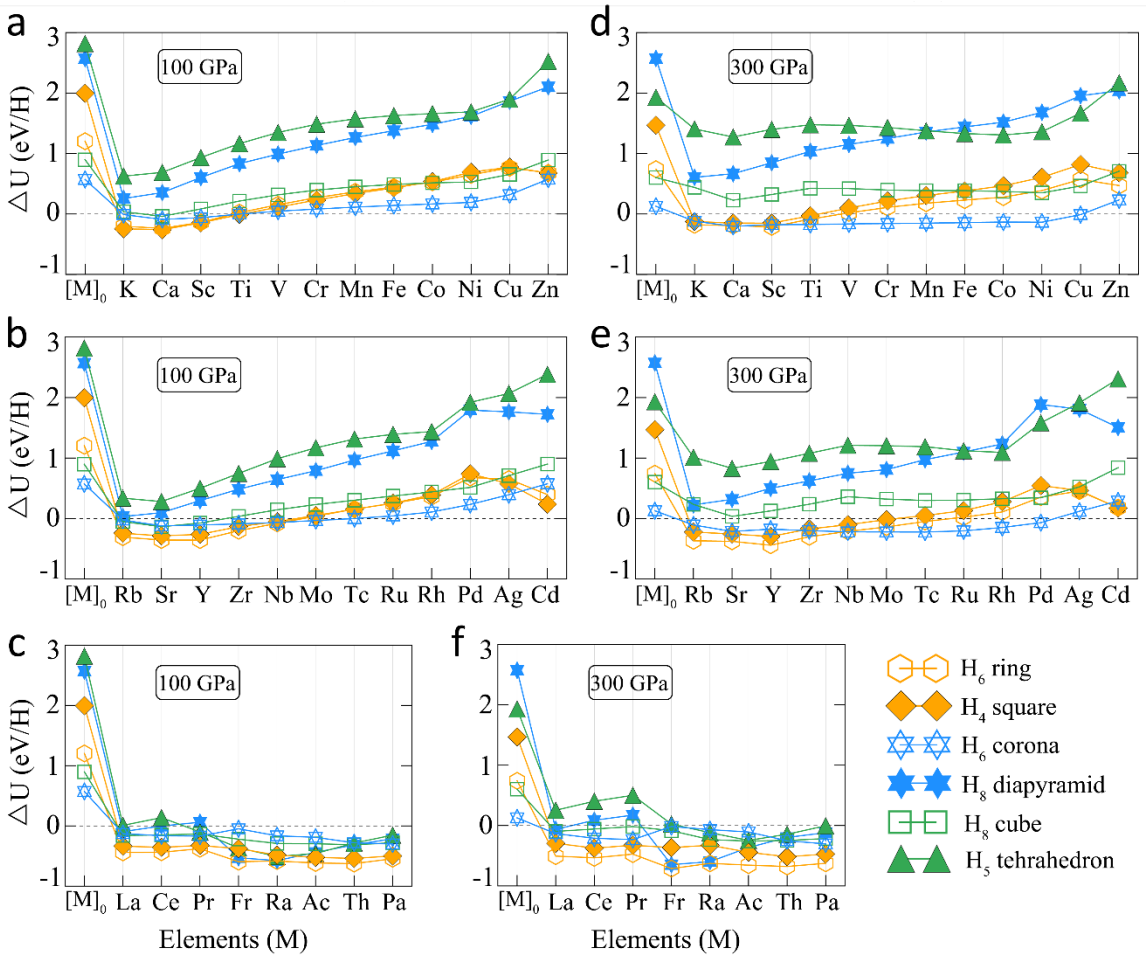

Fig. 4: The change of internal energies while forming H clusters in metal superhydrides. a-c, The energies of the H units relative to H_2 with the presence of metals in the 4th row (panel **a**), the 5th row (panel **b**) of periodic table and several rare earth metals (panel **c**), calculated by use of the He matrix at 100 GPa (see Methods). $[M]_0$ represents He matrix with no metals. **d-f**, The energies of the H units relative to H_2 with the presence of metals in the 4th row (panel **d**), the 5th row (panel **e**) of periodic table and several rare earth metals (panel **f**), calculated by use of the He matrix at 300 GPa.

Section VIII. Charge transfers in views of chemical bonds and chemical templates

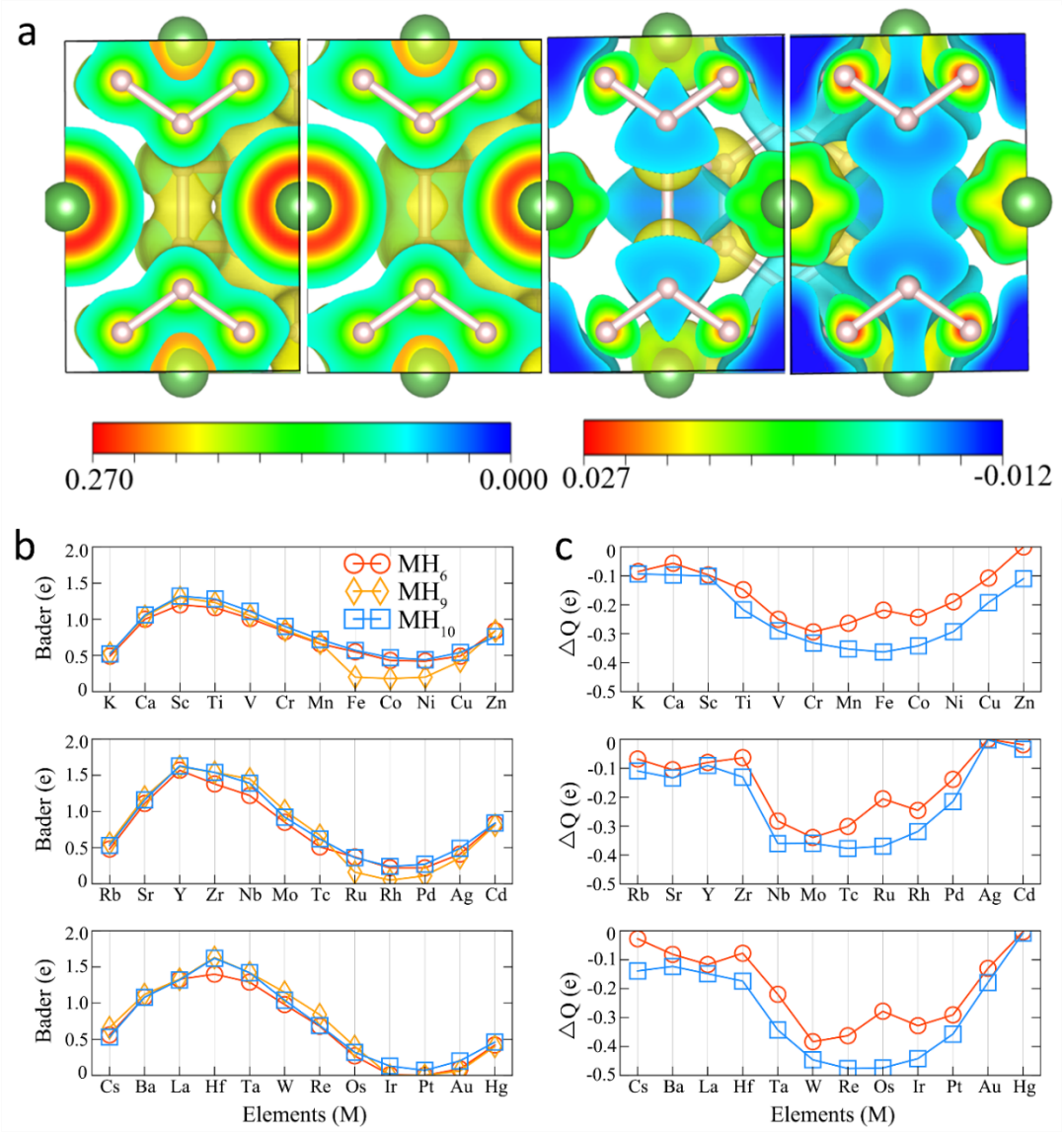

Fig. 5: The charge transfers calculated using free atoms or sub-lattices as the reference states. a, From left to right: the charge distribution of LaH_{10} [$\rho(LaH_{10})$] on (110) plane at 100 GPa; the summation of the charge distributions of La [$\rho(La)$] and H_{10} lattices [$\rho(H_{10})$] in LaH_{10} compound on (110) plane at 100 GPa; the difference between $\rho(LaH_{10})$ and $\rho(La) + \rho(H_{10})$ at 100 GPa; the difference between $\rho(LaH_{10})$ and $\rho(La) + \rho(H_{10})$ at 300 GPa. **b**, The Bader charges of MH_6, MH_{10} and MH_9 superhydrides for the 4th, 5th and 6th rows of metal elements. **c**, The integrated differential charge density of metals in MH_6, MH_{10} and MH_9 superhydrides (see Methods).

Section IX. The chemical templates and stability of mixed metal superhydrides

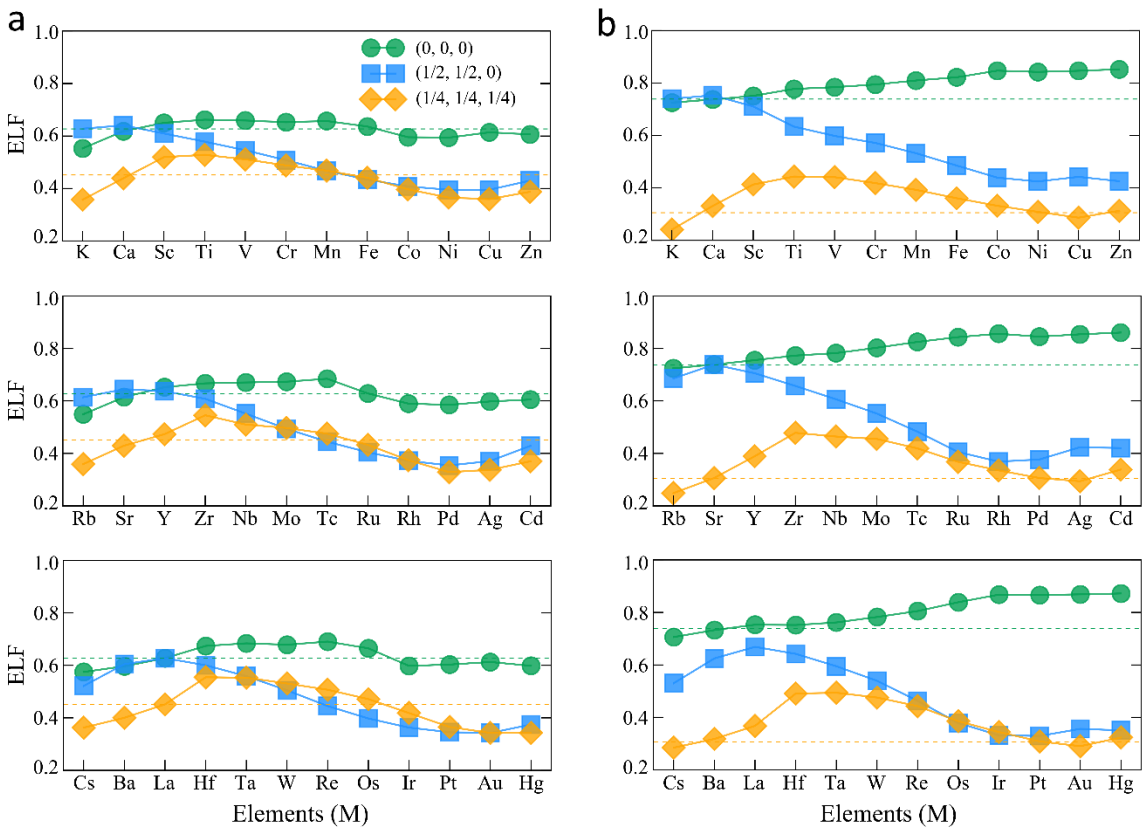

Fig. 6: The change of ELF values while replacing metals in MH_{10}. a, The change of ELF values at interstitial sites including (0, 0, 0), (1/2, 1/2, 0) and (1/4, 1/4, 1/4), while replacing one La atom in a conventional cell of LaH_{10} superhydrides at 100 GPa. M is a 4th, 5th, and 6th row metal element, respectively. The green and the orange dashed lines show the ELF values of La FCC at (0,0,0) and (1/4, 1/4, 1/4) points for comparison. **b**, The change of ELF values at interstitial sites including (0, 0, 0), (1/2, 1/2, 0) and (1/4, 1/4, 1/4), while replacing one Sr atom in a conventional cell of SrH_{10} superhydrides at 100 GPa. M is a 4th, 5th, and 6th row metal element, respectively. The green and the orange dashed lines show the ELF values of Sr FCC at (0,0,0) and (1/4, 1/4, 1/4) points for comparison.

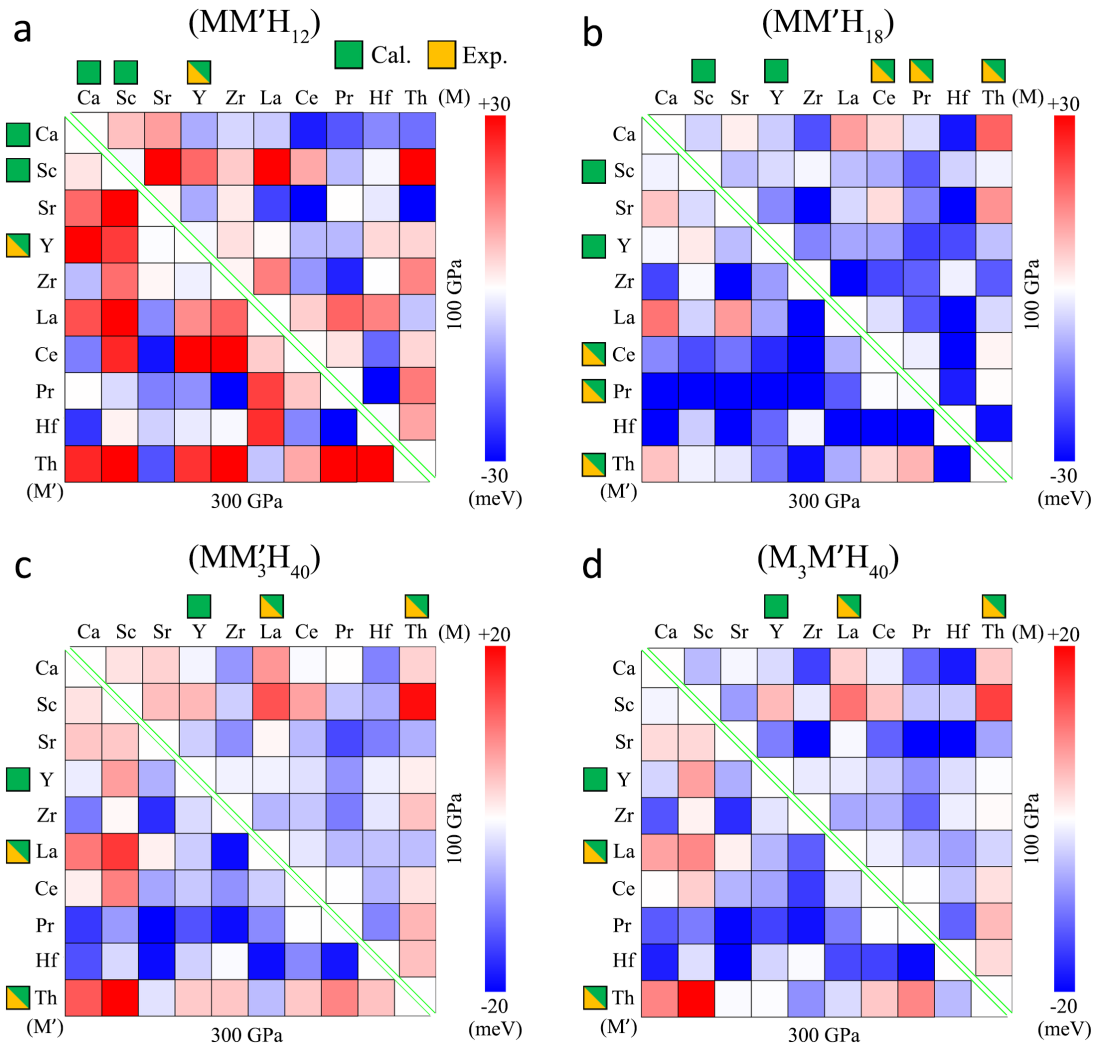

Fig. 7: The reaction enthalpies of two metal superhydrides with the same H lattice forming a mixed metal superhydrides. The formulas for calculating the reaction energies are shown in the Method section of the text. The energies are shown in meV per atom. Negative reaction enthalpies mean the mixed metal superhydrides are more stable. **a**, The reaction energies of forming $MM'H_{12}$ from MH_6 and $M'H_6$. **b**, The reaction energies of forming $MM'H_{18}$ from MH_9 and $M'H_9$. **c**, The reaction energies of forming MM'_3H_{40} from MH_{10} and $M'H_{10}$. **d**, The reaction energies of forming $M_3M'H_{40}$ from MH_{10} and $M'H_{10}$.

References

1. Wang, H., Tse, J. S., Tanaka, K., Iitaka, T. & Ma, Y. Superconductive sodalite-like clathrate calcium hydride at high pressures. *PNAS* **109**, 6463–6466 (2012).
2. Qian, S., Sheng, X., Yan, X., Chen, Y. & Song, B. Theoretical study of stability and superconductivity of ScHn (n=4-8) at high pressure. *Phys. Rev. B* **96**, 094513 (2017).
3. Abe, K. Hydrogen-rich scandium compounds at high pressures. *Phys. Rev. B* **96**, 144108 (2017).
4. Ye, X., Zarifi, N., Zurek, E., Hoffmann, R. & Ashcroft, N. W. High Hydrides of Scandium under Pressure: Potential Superconductors. *J. Phys. Chem. C* **122**, 6298–6309 (2018).
5. Troyan, I. A. *et al.* Anomalous high-temperature superconductivity in YH6. *arXiv:1908.01534 [cond-mat]* (2020).
6. Li, Y. *et al.* Pressure-stabilized superconductive yttrium hydrides. *Scientific Reports* **5**, 9948 (2015).
7. Geballe, Z. M. *et al.* Synthesis and Stability of Lanthanum Superhydrides. *Angewandte Chemie International Edition* **57**, 688–692 (2018).
8. Errea, I. *et al.* Quantum crystal structure in the 250-kelvin superconducting lanthanum hydride. *Nature* **578**, 66–69 (2020).
9. Liu, H., Naumov, I. I., Hoffmann, R., Ashcroft, N. W. & Hemley, R. J. Potential high-Tc superconducting lanthanum and yttrium hydrides at high pressure. *Proceedings of the National Academy of Sciences* **114**, 6990 (2017).
10. Peng, F. *et al.* Hydrogen Clathrate Structures in Rare Earth Hydrides at High Pressures: Possible Route to Room-Temperature Superconductivity. *Phys. Rev. Lett.* **119**, 107001 (2017).
11. Somayazulu, M. *et al.* Evidence for Superconductivity above 260 K in Lanthanum Superhydride at Megabar Pressures. *Phys. Rev. Lett.* **122**, 027001 (2019).
12. Semenok, D. V. *et al.* Superconductivity at 161 K in thorium hydride ThH10: Synthesis and properties. *Materials Today* **33**, 36–44 (2020).

13. Kvashnin, A. G., Semenok, D. V., Kruglov, I. A., Wrona, I. A. & Oganov, A. R. High-Temperature Superconductivity in a Th–H System under Pressure Conditions. *ACS Appl. Mater. Interfaces* **10**, 43809–43816 (2018).
14. Li, X. *et al.* Polyhydride CeH 9 with an atomic-like hydrogen clathrate structure. *Nature Communications* **10**, 3461 (2019).
15. Salke, N. P. *et al.* Synthesis of clathrate cerium superhydride CeH 9 at 80-100 GPa with atomic hydrogen sublattice. *Nature Communications* **10**, 4453 (2019).
16. Zhou, D. *et al.* Superconducting praseodymium superhydrides. *Science Advances* **6**, eaax6849 (2020).
17. Kruglov, I. A. *et al.* Uranium polyhydrides at moderate pressures: Prediction, synthesis, and expected superconductivity. *Science Advances* **4**, eaat9776 (2018).
18. Hooper, J., Terpstra, T., Shamp, A. & Zurek, E. Composition and Constitution of Compressed Strontium Polyhydrides. *J. Phys. Chem. C* **118**, 6433–6447 (2014).
19. Wang, Y., Wang, H., Tse, J. S., Iitaka, T. & Ma, Y. Structural morphologies of high-pressure polymorphs of strontium hydrides. *Phys. Chem. Chem. Phys.* **17**, 19379–19385 (2015).
20. Zhang, J. *et al.* High-temperature superconductivity in the Ti-H system at high pressures. *Phys. Rev. B* **101**, 134108 (2020).
21. Xiao, X. *et al.* Structure and superconductivity of protactinium hydrides under high pressure. *J. Phys.: Condens. Matter* **31**, 315403 (2019).
22. Xie, H. *et al.* Hydrogen 'penta-graphene-like' structure stabilized by hafnium: a high-temperature conventional superconductor. *arXiv:2001.04076 [cond-mat]* (2020).
23. Kruglov, I. A. *et al.* Superconductivity of LaH10 and LaH16 polyhydrides. *Phys. Rev. B* **101**, 024508 (2020).
24. Chen, W. *et al.* High-Pressure Synthesis of Barium Superhydrides: Pseudocubic BaH12. *arXiv:2004.12294 [cond-mat]* (2020).